Biosensors and Bioelectronics ■ (■■■■) ■■■–■■■

Contents lists available at ScienceDirect

Biosensors and Bioelectronics

journal homepage: www.elsevier.com/locate/bios

# Label-free detection of 3-nitro-L-tyrosine with nickel-doped graphene localized surface plasmon resonance biosensor

Siu Pang Ng [a], Guangyu Qiu [a], Ning Ding [a,b], Xiaoqing Lu [c], Chi-Man Lawrence Wu [a,b,*]

[a] Department of Physics and Materials Science, City University of Hong Kong, Hong Kong SAR, PR China
[b] Shandong Academy of Sciences, Jinan, Shandong 250014, PR China
[c] College of Science, China University of Petroleum, Qingdao, Shandong 266580, PR China

ARTICLE INFO

*Article history:*
Received 28 November 2015
Received in revised form
5 April 2016
Accepted 6 April 2016

*Keywords:*
Label-free biosensor
3-Nitro-l-tyrosine
Nickel-doped graphene
Localized surface plasmon resonance
Differential phase detection

ABSTRACT

3-nitro-L-tyrosine (3-NT) is believed to be a biomarker of neurodegenerative diseases and metal doped graphene possess exceptionally high binding energy of 3-NT with metal-nitro chemisorption. Here we report a novel label-free detection scheme of 3-NT via nickel-doped graphene (NDG) as the functionalized receptor on our phase detecting localized surface plasmon resonance (LSPR) biosensor. When compared with reported 3-NT immunoassay with enzyme-linked immunosorbent assay (ELISA), our NDG-LSPR platform offers two advantages i.e. 1) label-free and 2) capture of 3-NT by direct chemisorption. Our limit of detection for 3-NT in PBS was found to be 0.13 pg/ml and the linear dynamic range of response was from 0.5 pg/ml to 1 ng/ml, i.e. four orders of magnitude. The specificity of our NDG receptor to 3-NT was also verified with L-tyrosine of equivalent concentrations in PBS and diluted human serum, for which the NDG receptor shows negligible responses. In addition, the adsorption of 3-NT and L-tyrosine to the NDG receptor were also investigated by atomic force microscopy and further verified by surface enhanced Raman spectroscopy. Therefore, our NDG-LSPR biosensor competes favorably against ELISA and we believe it should be an attractive and economical solution to early diagnostic of 3-NT related disorders for clinical applications.

© 2016 Elsevier B.V. All rights reserved.

## 1. Introduction

3-nitro-L-tyrosine (3-NT) is believed to be a biomarker for protein tyrosine nitration, which is involved in the pathogenesis of various neurodegenerative diseases (Abello et al., 2009; Shu et al., 2014; Souza et al., 2008). Although existing method for the detection of 3-NT via liquid chromatography – tandem mass spectrometry (LC-MS/MS) demonstrates high sensitivity (Tsikas, 2010; Yi et al., 2000), it involves both expensive equipment and time consuming sample preparation. Thus, it is seldomly applied to early identification of patients with abnormal 3-NT level in clinical situations. On the other hand, the detection of 3-NT via enzyme-linked immunosorbent assay (ELISA) has demonstrated convincing capability of 3-NT detection to semi-picomolar level (Wayenberg et al., 2009). Generally, ELISA employs antibodies with tagged fluorescent dyes to produce measurement signal in the capture of corresponding antigens. However, there are a number of precautions in the deployment of antibodies in the field, e.g. storage temperature (Ciocca et al., 1983), contamination by preservatives (Ortiz de Montellano et al., 1988), and freeze-thaw cycling aggregation (Zhang et al., 2011). Therefore, ELSIA is rather restricted to laboratory operation. To tackle the issues on antibodies, synthetic receptors such as molecular imprinted polymers (MIP) (Mergola et al., 2013) were reported for biosensing of 3-NT with limit of detection (LOD) to 700 ng/ml. In comparison, the reported 3-NT concentration in healthy adults were determined to be about 2 nM in blood plasma (Tsikas, 2010) (i.e. approximately 0.45 ng/ml with molecular weight of 226.19 g/mole of 3-NT). Patients with Alzheimer's disorders (Tohgi et al., 1999) and diabetes (Ceriello et al., 2001) possess 3-NT, which is 6–300 times of that of a healthy control (i.e. 2.7–135 ng/ml). Obviously, the reported MIP receptor with high-pressure liquid chromatography (HPLC) is insufficient to identify these patients with 3-NT level less than the LOD in blood plasma. For non-invasive detection of 3-NT in urine, the 3-NT concentration drops further to pg/ml (Chao et al., 2015), so that the reported MIP with HPLC technique is not able to cope with such ultra-sensitive detection. Therefore, alternative synthetic 3-NT receptor to MIP with improved LOD needs to be investigated. The LODs of 3-NT by various techniques are included in Supplementary Table S1.

* Corresponding author at: Department of Physics and Materials Science, City University of Hong Kong, Hong Kong SAR, PR China.
*E-mail address:* lawrence.wu@cityu.edu.hk (C.-M. Wu).

http://dx.doi.org/10.1016/j.bios.2016.04.017
0956-5663/© 2016 Elsevier B.V. All rights reserved.

Recently, the renaissance of label-free immunoassay biosensors, i.e. surface plasmon resonance (SPR) (Homola, 2008) and localized surface plasmon resonance (LSPR) via plasmonic nanostructures (Mayer and Hafner, 2011), have demonstrated excellent sensitivity in detection of various pathogens. However, biosensing with these devices generally depends on surface functionalization with antibodies (Guo and Kim, 2012), thus the inherent restrictions stated previously need to be observed. In contrast, the emergence of two dimensional (2D) materials, i.e. graphene and graphene oxides, as sensing receptor has gained much attention (Georgakilas et al., 2012) owing to their ability to bind to the aromatic-ring amino acids of proteins via π-π interaction (Liu et al., 2012). We have explored the detection of 3-NT with metal-doped graphene materials using density functional theory (DFT) by computer simulation (Ding et al., 2012). It was found that the metal-doped graphene favors chemical adsorption of 3-NT molecules by forming the metal-nitro bond, whereas the physical adsorption of 3-NT molecules on pristine graphene is much weaker than its metal doped counterpart. It was also found that nickel-doped graphene (NDG) possesses higher binding energy to 3-NT than doping with other metal elements. Therefore, the above-mentioned computational results indicated that biosensing of 3-NT with NDG may be feasible. However, there is a well-known limitation on the molecular weight of specimen detectable via SPR biosensor, i.e. 200 g/mol (Myszka, 1997). This is very close to the molecular weight of 226.19 g/mol of 3-NT, which means that the detection of 3-NT with conventional SPR biosensor is rather difficult. On the contrary, LSPR biosensors with nanostructures enhancement seem to offer better performance in detecting small biomolecules than its SPR predecessor (Zeng et al., 2014). Inspired by the DFT computation and concept on graphene enhancement to plasmonic biosensor (Wu et al., 2010), we incorporated the NDG receptor to our established phase detecting LSPR biosensor with self-assembly gold nanoislands (Qiu et al., 2015) and performed label-free detection of 3-NT to demonstrate the sensitivity, specificity and dynamic range of the NDG-LSPR biosensor. We have also examined the π–π stacking interaction (Martinez and Iverson, 2012) between 3-NT (Ding et al., 2012) and L-tyrosine (Rajesh et al., 2009) on pristine and NDG respectively. It was found the adsorption energy with parallel aromatic π stacking orientation (R-site as in Supplementary Fig. S1) was unfavorable comparing to orthogonal chemisorption via the metal-nitro bond ($NO_2$-site as in Fig. S1). Our finding of −0.16 eV was in agreement with the relatively weak adsorption energy of −0.31 eV between L-tyrosine and pristine graphene in reported previously by Rajesh et al. (2009). Therefore, it is believed that the π–π stacking interaction is trivial for the capture of 3-NT molecule on the NDG receptor and so the interaction will not be discussed further. We have also calculated the adsorption energy of 3-NT and L-tyrosine on the NDG structure. It was found that the adsorption energy due to chemisorption via the $NO_2$ site of 3-NT on NDG is −1.46 eV, whereas that via $NH_2$ site of L-tyrosine is only −1.08 eV (Supplementary Table S3). This is similar to the work of Luo et al. (2013) in which NDG showed high adsorption energy of about −4 eV to L-cysteine while pristine graphene showed unfavorable adsorption energy of about 1 eV. This is believed to be the reason for NDG only selective for 3-NT instead of other biomolecules present in human serum.

## 2. Materials and methods

### 2.1. Materials

3-Nitro-L-tyrosine crystalline (3-NT, purity ≥98%), L-tyrosine (purity ≥99%), and nickel (II) chloride hydrate ($NiCl_2$•$6H_2O$, 99.95% trace metals basis) were purchased from Sigma-Aldrich (Saint Louis, USA). Both 3-NT and L-tyrosine were diluted with phosphate buffered saline (PBS, Sigma-Aldrich, pH 7.4 at 25 °C, containing 0.138 M NaCl; 0.0027 M KCl) to required concentrations, the PBS solution was also employed as the running buffer in our experiments. Human serum from male AB plasma and sterile-filtered (#H4522-20 ml) was also acquired from Sigma-Aldrich for real sample testing. Pristine graphene monolayer flakes dispersed in ethanol with concentration of 1 mg/L was purchased from Graphene Laboratories Inc. (New York, USA). Ethanol of analytical grade was also purchased from Sigma-Aldrich as solvent for nickel chloride hydrate. Deionized water of 18.2 MΩ cm was used whenever necessary. All chemicals were used without further purification. BK7 glass slides were purchased from Edmund Optics Inc. (New Jersey, USA).

### 2.2. Synthesis of nickel-doped graphene on self-assembly gold nanoislands

There are three essential steps to fabricate the NDG-LSPR biosensing chip in sequence, 1) synthesis of the self-assembly gold nanoislands (SAM-AuNIs) on BK7 slides, 2) veiling of graphene on SAM-AuNIs, 3) nickel-doping of the graphene sheets. In the first step as shown in Scheme 1a and b, the BK7 glass slides (35 mm × 25 mm × 2 mm) were initially sonicated in deionized water (DW) and ethanol (Sigma-Aldrich) to remove contaminants. The glass slide was dried subsequently in nitrogen atmosphere and a gold film of 5 nm nominal thickness was evaporated by magneto sputtering. Then, as shown in Scheme 1b, the gold-coated glass was thermally annealed at 550 °C for 3 h in air to form the gold nanoislands in self-assembly fashion (Qiu et al., 2015). The fabrication parameters, i.e. the initial nominal thickness, annealing temperature, and annealing duration were optimized for the best refractive index resolution according to our previous experience. In the second step as shown in Scheme 1c, graphene dispersed in ethanol was spin-coated onto the SAM-AuNIs chip at 2000 rpm for 15 s. Then, the graphene on SAM-AuNIs chip was thermally annealed at 400 °C for 2 h with continuous flow of 800 sccm Argon gas to prevent oxidation of the graphene sheet (Xu et al., 2013). This step will be referred as thermal veiling of graphene, which improves the contact between the SAM-AuNIs and the graphene sheets. After natural cooling in Argon gas, the graphene veiled SAM-AuNIs chip was ready for doping with nickel. In the third step as shown in Scheme 1d, $NiCl_2$•$6H_2O$ of about 0.1 mM in ethanol was spin-coated onto the chip and annealed again at 500 °C for 30 min with the same flow rate of Argon gas (Lee et al., 2013). It is worth to note that Lee et al. reported that 10, 100, and 200 mM of nickel chloride solution produced nickel nanoparticles size of about 4 nm which are too large for 3-NT adsorption according to our computation model as illustrated in the supplementary Fig. S1 with scale of 1 nm (Ding et al., 2012). Therefore, we had deliberately reduced the concentration of the nickel dopant by three orders of magnitude in comparison to Lee et al. This was done to reduce the size of the nickel nanoparticle dopants on graphene. We had also tested the nickel dopant concentration from 0.01 to 1 mM for sensing of 3-NT (data not shown) and the optimal concentration was found to be 0.1 mM. After the completion of the above steps, the NDG-LSPR chip was ready for installation and detection, as shown in the white-light interferometer setup with optical components labelled in Scheme 1e.

### 2.3. Detection procedure

The common-path white-light interferometric system (Loo et al., 2014; Ng et al., 2013) and differential phase detecting method (Ng et al., 2010, 2011; Qiu et al., 2015) were utilized to

Please cite this article as: Ng, S.P., et al., Biosensors and Bioelectronics (2016), http://dx.doi.org/10.1016/j.bios.2016.04.017

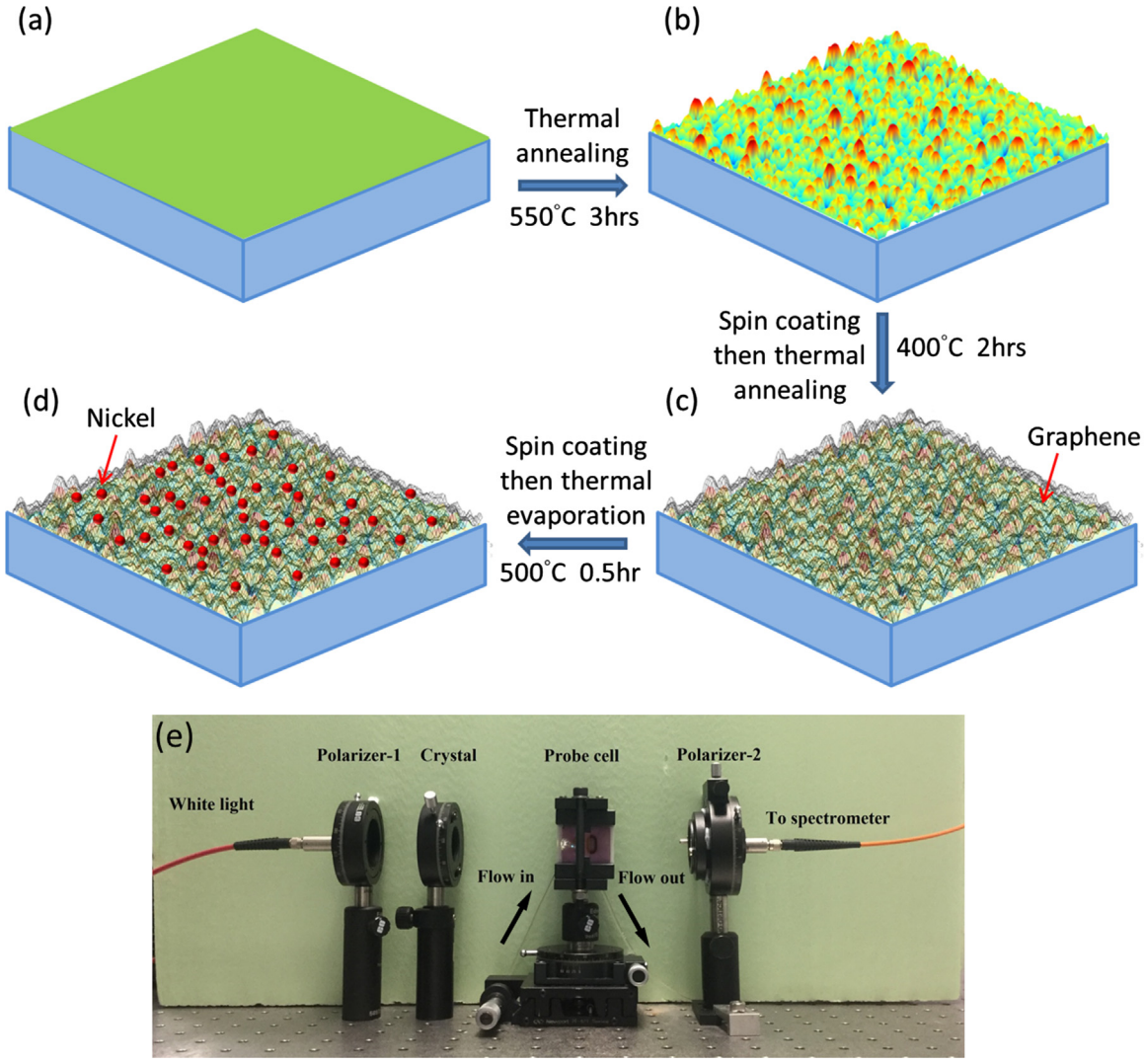


**Scheme 1.** Schematic illustration of the fabrication procedure of the NDG-LSPR chip, i.e. (a) sputtering of an ultrathin layer of gold of nominal thickness 5 nm, (b) formation of the SAM-AuNIs by thermal annealing at 550 °C for 3 h in air, (c) spin-coating and thermal veiling to immobilize graphene flakes to the SAM-AuNIs, (d) spin-coating of $NiCl_2$•$6H_2O$ solutions and thermal evaporation to dope the graphene flakes with nickel, (e) white-light interferometer for installation of the NDG-LSPR chip and detection of 3-NT molecules.

perform the label-free detection of 3-NT with the NDG-LSPR biosensor. A white-light LED source (LedEngin, LZ1-00W00), with emission spectrum from 480 nm to 730 nm and bandwidth of 150 nm, was linearly polarized with a broadband polarizer (Edmund Optics, #89-602). A birefringent crystal was added into the light path so that sufficient retardation was introduced to the s-and p-polarized components. Then, a right-angle BK7 prism was used to couple the evanescent field of the incident light with the SAM-AuNIs on total internal reflection (TIR). The probe cell consisted of an airtight flow chamber which was secured to the functionalized SAM-AuNIs chip and coupled to the BK7 prism by optical coupling fluid (AL-5252, AngstromLink). No further functionalization steps were needed for the setup and the PBS buffer was allowed to flow across the chamber to establish the steady baseline of phase signal prior to the injection of 3-NT solutions. At the end of the optical path, a high resolution temperature stabilized spectrometer (Avantes, AvaSpec-ULS2048LTEC) covering 500–750 nm with resolution of 0.2 nm was used to capture the interference signal from the probe cell. Finally, the windowed Fourier transforms (WFT) method was applied to retrieve the phase information from the interference spectrum in real time. The phase data in correlation with the 3-NT concentration was extracted from the signals by mutual subtraction with the initial phase reference.

## 3. Results and discussion

### 3.1. Detection of 3-NT and L-tyrosine by NDG-LSPR biosensor

Initial 3-NT solution was prepared by dissolving 1 g of 3-NT crystalline into 1 l of PBS buffer to obtain the concentration of 1 mg/ml. Then, 1 ml of the seeding 3-NT solution was added to 999 ml of PBS buffer, so that the 3-NT concentration was reduced to 1 μg/ml. The same procedure was repeated twice so that the 3-NT solutions with concentration of 1 ng/ml and 1 pg/ml were obtained respectively. Similarly, by adding 1 ml of 3-NT solution of concentration 1 ng/ml to 9 ml and 99 ml of PBS buffer, 3-NT concentrations of 100 pg/ml and 10 pg/ml were obtained respectively. Further, by adjusting the volume of PBS buffer, 3-NT solutions of 0.1 pg/ml, 0.3 pg/ml, 0.5 pg/ml and 0.8 pg/ml were prepared. As parts of the experiment was to test the specificity, L-tyrosine solutions of 0.1 pg/ml, 10 pg/ml and 1 ng/ml were prepared in a similar fashion. PBS running buffer was also used to determine the

Please cite this article as: Ng, S.P., et al., Biosensors and Bioelectronics (2016), http://dx.doi.org/10.1016/j.bios.2016.04.017

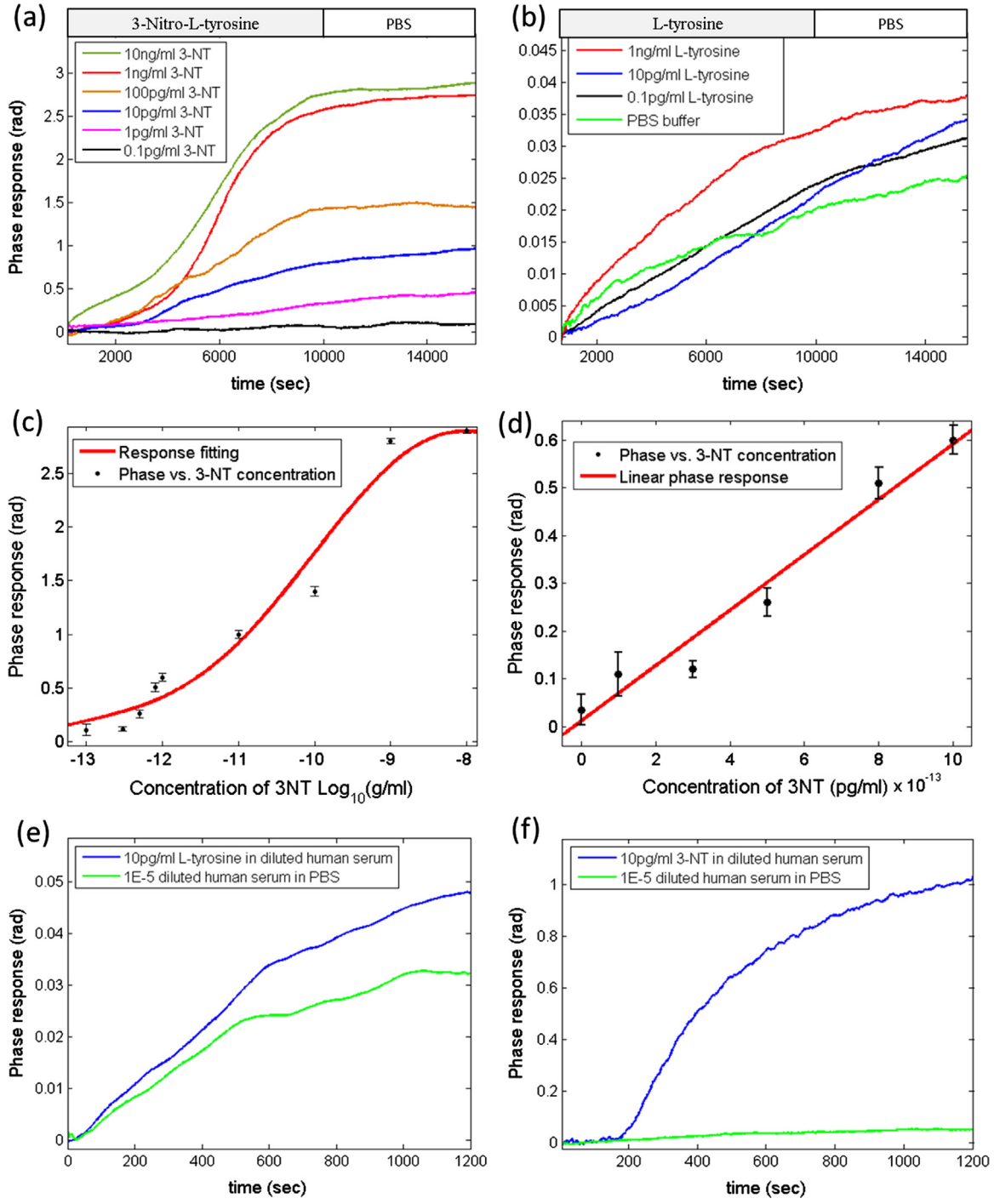


**Fig. 1.** (a) Phase sensorgram of 3-NT of various concentrations in PBS buffer, (b) sensorgram of L-tyrosine of selected concentrations and that of PBS control, (c) logarithmic response curve of 3-NT from 0.1 pg/ml to 10 ng/ml, (d) estimation of the 3-NT LOD by linear regression, (e) sensorgram of 1E-5 diluted human serum in PBS and 10 pg/ml of L-tyrosine in diluted serum, (f) sensorgram of 10 pg/ml 3-NT in dilute serum.

stability of the system. A peristaltic pump (Reglo Digital, Ismatec) was employed to inject all samples at a constant flow rate of 5 µl/min.

The real-time phase data of 3-NT in various concentrations are shown in Fig. 1a and those of L-tyrosine in similar concentrations are presented in Fig. 1b respectively. Since the NDG receptors directly capture the 3-NT molecules, no further functionalization was attempted on the NDG-LSPR chip. Before injection of the 3-NT and L-tyrosine solutions, PBS buffer was allowed to flow across the chamber for 1 h to establish a steady baseline (data not shown). At the beginning, 3-NT solutions from 0.1 pg/ml to 1 ng/ml in increment of ten folds were injected one at a time and the maximum tested concentration was 1 µg/ml. For the first 5000 s, the phase response of the NDG-LSPR biosensor increased steadily and the maximum phase value was attained at about 10,000 s. It was found that the higher the 3-NT concentration, the steeper the slope of the phase increment and the larger the final phase value obtained by the sample. By observation, the trend of the 3-NT conjugation on NDG receptor by phase detection is similar to our previous immunoassay of cytochrome *c* using DNA aptasensor (Loo et al., 2014). To verify the binding of 3-NT to the NDG receptor, PBS buffer was injected from 12,000 to 15,000 s. Fig. 1a

shows that no phase change was observed after rinsing with PBS. This is an indication that 3-NT molecules were adsorbed to the NDG receptors. Contrary to Fig. 1a, the phase response of L-tyrosine adsorption on the NDG receptor differed entirely as shown in Fig. 1b. Although the concentration of L-tyrosine increased from 0.1 pg/ml to 10 pg/ml and finally to 1 ng/ml in a total duration of 12,000 s, the corresponding phase values merely increased to 0.023, 0.024 and 0.033 rad, respectively. For the same concentrations of 3-NT, the phase values were 0.063, 0.330 and 2.576 rad, respectively. Therefore, the phase responses of the NDG receptor to 3-NT are 3, 14 and 78 folds over those of L-tyrosine of the same concentration, suggesting that the specificity of the NGD receptor may be adequate in differentiating the two molecules. The phase drift due to running PBS buffer also attained 0.020 rad after 12,000 s, as shown in Fig. 1b, and it was about the same level as that of L-tyrosine. We believe the drift was due to temperature fluctuation as the experiments were performed without special temperature control. Therefore, isothermal conditioning of the flow chamber and solutions may be necessary to improve the sensitivity at sub pg/ml level. It is also important to differentiate our NDG-LSPR biosensing of 3-NT from that reported previously via SPR (Jin et al., 2011). First, our synthetic NDG receptor plays the role of 3-NT antibody and has demonstrated high specificity to 3-NT molecule in differentiating it from L-tyrosine. Secondly, the SAM-AuNIs functions as the plasmonic nanostructure for sensing of localized refractive index alteration due to 3-NT and NDG conjugation. This is different from the gold film based Spreeta 2000 device used by Jin et al. Thirdly, our detection scheme is based on differential spectral phase measurement which is known to deliver superior sensitivity than the intensity acquisition scheme. In combination of these three advantages, we believe our NDG-LSPR biosensor should outperform those reported with SPR for 3-NT detection.

For verification with real samples, human serum was diluted to 1/100,000 in PBS (i.e. 1E-5) to avoid refractive index alteration between the sample and running buffer, then 10 pg/ml of 3-NT and L-tyrosine were added to the diluted serum for testing. We have increased the flow rate to about 50 μl/min, so that the test duration was reduced to merely 1200 s. The results of L-tyrosine and 3-NT in diluted serum are shown in Fig. 1e and f, respectively. The result of diluted serum is also included for comparison. Fig. 1e shows that the phase response of diluted serum had attained 0.033 rad. This is larger than the value of 0.025 rad of the PBS in Fig. 1b, assuming that the same volume of fluid had passed over the flow chamber. With the addition of 10 pg/ml of L-tyrosine to the diluted serum, the phase response increased to 0.048 rad, as shown in Fig. 1e. However, after adding 10 pg/ml of 3-NT, as shown in Fig. 1f, the phase response increased dramatically to 1.02 rad. The phase sensorgram also attains typical response of kinetic binding as described by Homola (Homola, 2008). When comparing Fig. 1e with f, we are convinced that the NDG receptor is practical for detecting and differentiating 3-NT and L-tyrosine in the serum samples.

The variation of phase response with 3-NT concentrations over the range 0.1 pg/ml–10 ng/ml is shown in the logarithmic plot of Fig. 1c. The data used to estimation the limit of detection (LOD) are included in the linear plot in Fig. 1d. Each concentration in Fig. 1c and d was repeated for at least 3 times to determine the standard deviation. When the 3-NT concentration exceeded 1 ng/ml, the NDG-LSPR phase response of the optimal resonance wavelength started to saturate at about 2.763 rad. It indicates that most of the NDG receptors on the SAM-AUNIs were occupied by the 3-NT molecules. Therefore, further increase in the 3-NT concentration can no longer produce any phase response. Thus, the linear dynamic range of our NDG-LSPR biosensor was determined from Fig. 1c and it is estimated to be from 0.5 pg/ml to 1 ng/ml. In order to estimate the limit of detection (LOD), linear curve fitting was applied to the sub pg/ml (i.e. $\leq 10 \times 10^{-13}$ g/ml) concentrations. The linear equation was found to be $y = 5.797 \times 10^{11}x + 0.01165$ (R-square = 0.9649), as shown in Fig. 1d. This equation was used to calculate the LOD as defined by IUPAC (International Union of Pure and Applied Chemistry). According to IUPAC, the system response at the LOD should be the sum of the averaged blank measures, i.e. 0.032 rad with PBS buffer, and triple of its standard deviation, i.e. $3 \times (1.5 \times 10^{-2})$ rad. Based on the above calculation, the uncertainty of our NDG-LSPR system is $(0.032) + 3 \times (1.5 \times 10^{-2}) =$ 0.078 rad. Then, this value was substituted into the $y$ of the linear equation to calculate $x$, which is known as the LOD. Thus, our LOD was calculated to be $\geq 0.1345$ pg/ml. In comparison with previous results for 3-NT detection with SPR biosensor for which the LOD was reported as 4.7 ng/ml (Jin et al., 2011), our system has improved the LOD by four orders of magnitude. It is therefore clear that the label-free detection of 3-NT with our NDG-LSPR phase detecting biosensor had achieved the sub pg/ml level. We believe this is a significant advancement for clinical applications as healthy individuals usually possess about $63.2 \pm 51.5$ pg/ml urinary 3-NT in concentration (Chao et al., 2015). Therefore, rapid and non-invasive 3-NT detection with our NDG-LSPR biosensor is certainly practical. A brief summary of LOD of previous works in 3-NT detection is given in Table S1.

### 3.2. Adsorption of 3-NT and L-tyrosine to NDG by atomic force microscopy

With significant improvement of detecting 3-NT via our label-free NDG-LSPR biosensor, it would be rather interesting to examine the nanostructures of these NDG receptors as well as to visualize the morphological change due to adsorption of 3-NT and L-tyrosine molecules respectively. This was done using atomic force microscopy (AFM) with the objectives of: 1) to visualize the formation of the SAM-AuNIs before and after the first thermal annealing process, 2) to ensure the graphene flakes survived the second thermal annealing process, i.e. graphene thermal veiling, and 3) to investigate the effect of nickel-doping on the morphology of graphene veiled SAM-AuNIs. A Veeco Nanoscope V® AFM scanner was employed to perform the experiment. The results are shown in Fig. 2. In order to visualize the SAM-AuNIs, a 1 μm square area of the bare gold surface is plotted in Fig. 2a; its root-mean-square surface roughness (Rq) (DeGarmo, 2003) was calculated as 0.64 nm. After the first thermal annealing process, Rq increased from 0.64 to 9.14 nm, which is in agreement with the formation of SAM-AuNIs shown in Fig. 2b. By spin coating and thermal veiling of graphene flakes, the surface morphology changed considerably as shown in Fig. 2c. We have selected an area to visualize the change. In the lower left of Fig. 2c, there are unveiled SAM-AuNIs with distinctive gaps among themselves. At the center of Fig. 2c, there are SAM-AuNIs covered by single layer of graphene flakes. In the upper right of Fig. 2c, the SAM-AuNIs are veiled by multiple layers of graphene flakes and the nanoisland features were found to diminish. Rq at the center of Fig. 2c also decreased from 9.14 to 7.88 nm. Further doping by nickel ions reduces Rq further to 5.62 nm, as shown in Fig. 2d. Since the nickel ion concentration was merely 0.1 mM which is too low to form large nanoparticles of the same size as SAM-AuNIs, nickel nanoparticles are invisible in the AFM scan. Nevertheless, the reduction of the Rq value still reveals the morphological change due to nickel-doping.

After conducting the immunoassay experiments, NDG-LSPR chips for both 3-NT and L-tyrosine with concentration of 1 ng/ml were scanned by AFM and the results are shown in Fig. 3. The adsorption of 3-NT on the NDG receptor over the SAM-AuNIs provided an overall effect of a flattened AFM scan. On the other hand, the adsorption of L-tyrosine was insignificant as the

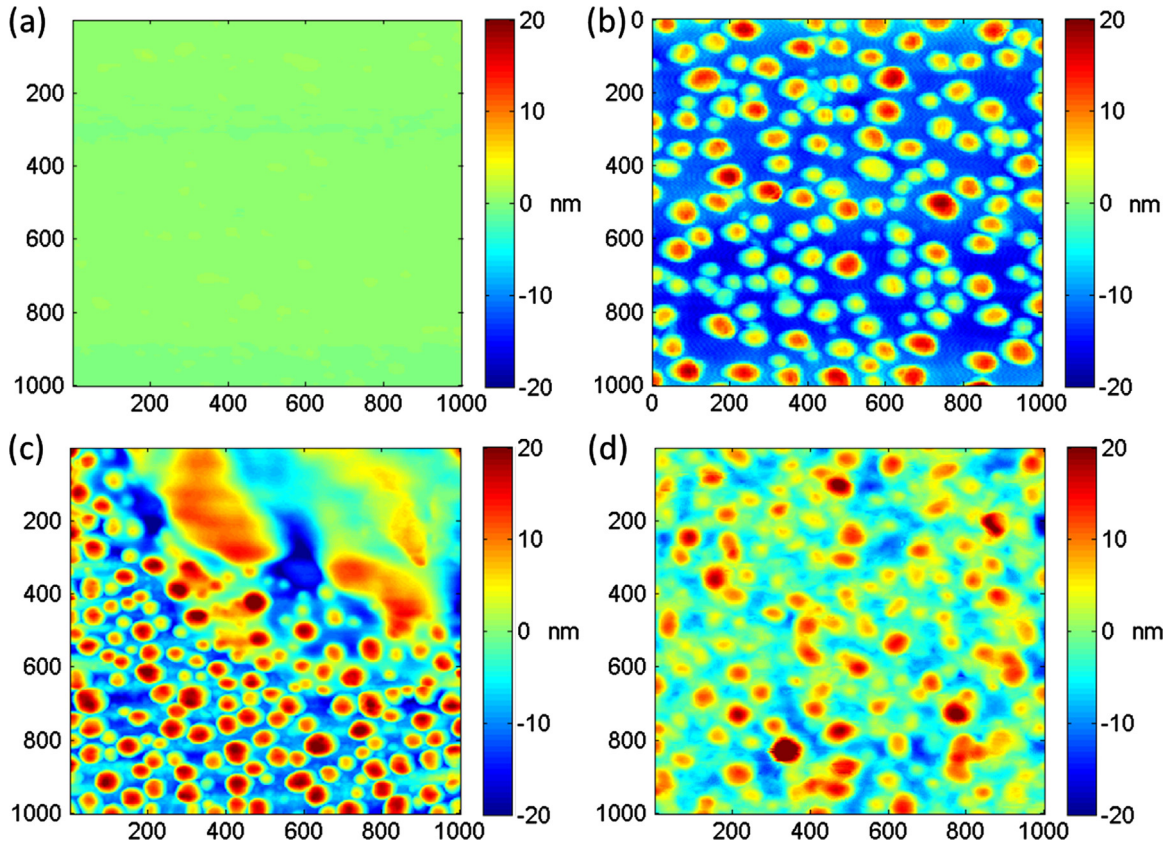


**Fig. 2.** AFM scan of (a) bare gold film as sputtered, (b) after formation of the SAM-AuNIs, (c) thermally veiled graphene flasks on the SAM-AuNIs in the top right corner and unveiled SAM-AuNIs in the lower left, (d) nickel-doped graphene on the SAM-AuNIs.

graphene veiled SAM-AuNIs are still visible with isolated gaps among themselves. The Rq values are 3.29 nm and 5.42 for Fig. 3a and b respectively. It is believed that chemisorption of 3-NT to the NDG receptor contributed to the reduction of surface roughness but there was no such conjugation for L-tyrosine. Therefore, Rq is reduced from 5.62 nm (Fig. 2d) to 3.29 nm (Fig. 3a) for 3-NT, whereas Rq remains almost the same as 5.42 nm (Fig. 3b) for L-tyrosine. A table of the Rq values for each AFM scan is included in Supplementary Table S2.

### 3.3. *Characterization by surface enhanced Raman spectroscopy*

Although the AFM scans in the previous section suggest that graphene flakes were successfully immobilized onto the SAM-AuNIs, stacking of graphene flakes was also observed. As a result, nickel-doping on graphene as well as adsorptions of 3-NT and L-tyrosine onto the NDG receptor could not be visualized by AFM. Therefore, we addressed these uncertainties by measuring the surface enhanced Raman scattering (SERS) of these samples. SERS is a well-known technique to provide finger-print identification of various chemical elements at microscopic scale (Schlücker, 2014). Since the SAM-AuNIs are inherent plasmonic nano-antennas, they also participate in electromagnetic (EM) enhancement of SERS by confining the incident laser light. We aimed to acquire the Raman signature of graphene on the SAM-AuNIs so that we could predict its layer structure and access its quality. Thus, we performed streamline Raman mapping of selected areas of 60 μm square on the samples using a Renishaw inVia® confocal Raman microscope with a 50 × objective, 633 nm laser of 1 mW incident power and integration time of 2 s. The results of Raman shift from 1000 $cm^{-1}$

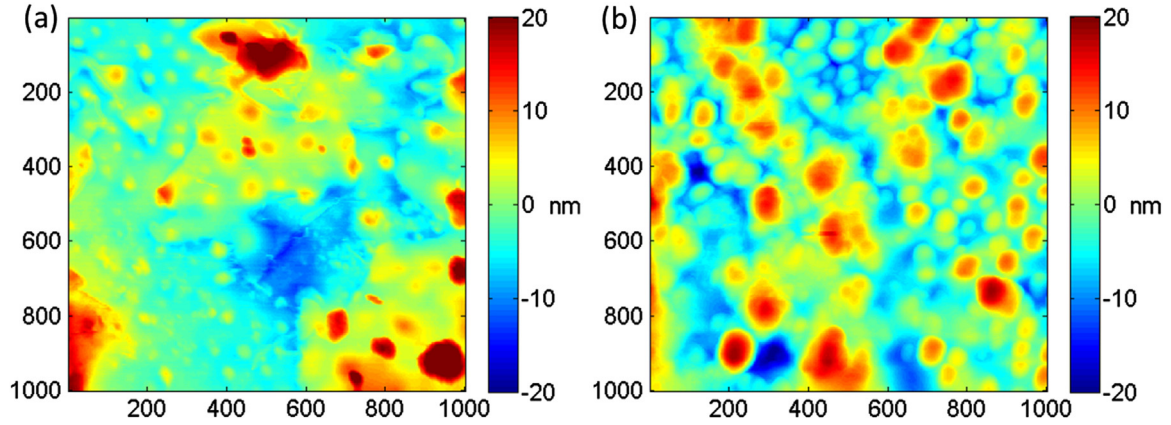


**Fig. 3.** AFM scan of (a) 1 ng/ml 3-NT on the NGD-LSPR chip after immunoassay, (b) L-tyrosine of the same concentration on the NDG-LSPR chip.

Please cite this article as: Ng, S.P., et al., Biosensors and Bioelectronics (2016), http://dx.doi.org/10.1016/j.bios.2016.04.017

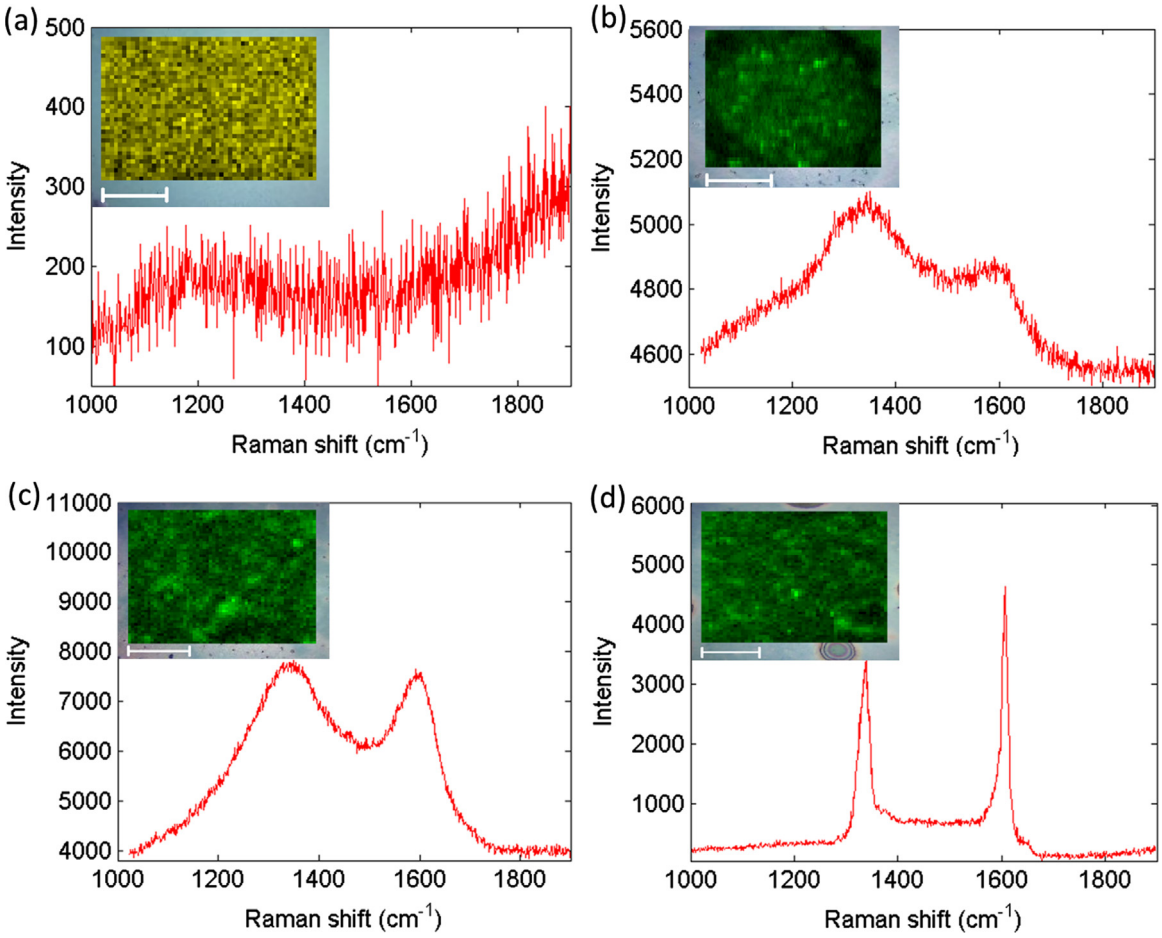


**Fig. 4.** SERS of (a) bare SAM-AuNIs with inserted pseudo map at 1598 $cm^{-1}$, (b) graphene flakes on SAM-AuNIs before annealing with inserted pseudo map at 1598 $cm^{-1}$, (c) graphene veiled on SAM-AuNIs after annealing with inserted pseudo map at 1598 $cm^{-1}$, (d) nickel-doped graphene on SAM-AuNIs after soaking and thermal evaporation with inserted pseudo map at 1608 $cm^{-1}$. Scale bar of the pseudo maps is 20 μm.

to 1850 $cm^{-1}$ are shown in Fig. 4. In Fig. 4a, the bare chip with SAM-AuNIs shows no peak in the spectral range of interest, and the intensity of 1598 $cm^{-1}$ was selected to reconstruct the pseudo map in the inset of Fig. 4a. Since graphene was absent, the map appears random. The scale bars in all insets are 20 μm. After spin coating of graphene flakes, two peaks at 1350 $cm^{-1}$ and 1598 $cm^{-1}$ appears in Fig. 4b. These two peaks can be assigned to the D- and G-band of the vibrating $sp^3$ and $sp^2$ carbon atoms respectively (Gao et al., 2010; Zhang et al., 2014). After thermal veiling, the D- and G-band of the graphene signature survived in Fig. 4c, indicating the presence of graphene flakes on the sample. With further nickel-doping, the two peaks still present, as shown in Fig. 4d, but the G-band has redshifted from 1598 $cm^{-1}$ to about 1608 $cm^{-1}$. This is in agreement with nickel-doping performed by Lee et al. who also reported redshifted of the G-band (Lee et al., 2013). The pseudo maps of G-band at 1598 $cm^{-1}$ are reconstructed as inset of Fig. 4b and c, and that of 1608 $cm^{-1}$ is placed in Fig. 4d. The pseudo maps in Fig. 4b, c and 4d appear quite different from that of Fig. 4a as there are numerous bright spots of the G-band signature in these maps. Therefore, we believe NDG were present on our biosensing chips.

Finally, we employed the same procedure but increased the incident laser power to 10 mW to investigate the adsorption of 3-NT and L-tyrosine on the NDG-LSPR chips after conducting the immunoassay. The SERS spectra and pseudo maps of the two molecules on the NDG-LSPR chip are shown in Fig. 5. It is important to state that the 3-NT solution of 100 pg/ml was used to construct Fig. 5a and b, whereas L-tyrosine solution of 1 ng/ml was needed to obtain Fig. 5c and d. We believe that the relatively poor absorption of the L-tyrosine molecules to the NDG receptor is the reason for the tenfold concentration increment. The dominating 3-NT peak appears at 1335 $cm^{-1}$, which is in good agreement with that reported by McNay et al. (2011). The pseudo map of the dominating peak is reconstructed in Fig. 5b and granular distribution of the bright patches indicates abundant adsorption of 3-NT molecules onto the NDG receptors. On the other hand, the L-tyrosine spectrum in Fig. 5c shows much weaker signal than those of 3-NT of Fig. 5a despite the L-tyrosine concentration was ten folds on 3-NT on the chip. Several dominating peaks were identified. The peak at 1590 $cm^{-1}$ may be due to in-plane C–C stretching (Grace et al., 2002) of the aromatic ring. The pseudo map of the chosen peak in Fig. 5d reveals rather random distribution of the signal that is different from those of Fig. 5b. We believe that the absorption of L-tyrosine by the NDG receptors is rather random. Thus, the SERS data supports our claim that the NDG receptor is highly specific to the 3-NT molecules in comparison with L-tyrosine.

## 4. Conclusions

We have successfully demonstrated a novel label-free biosensor with nickel-doped graphene synthetic receptor for detection of 3-NT biomarkers in aqueous PBS solution and diluted human serum, with good specificity. When combined with differential phase detecting LSPR configuration, we have significantly

Please cite this article as: Ng, S.P., et al., Biosensors and Bioelectronics (2016), http://dx.doi.org/10.1016/j.bios.2016.04.017

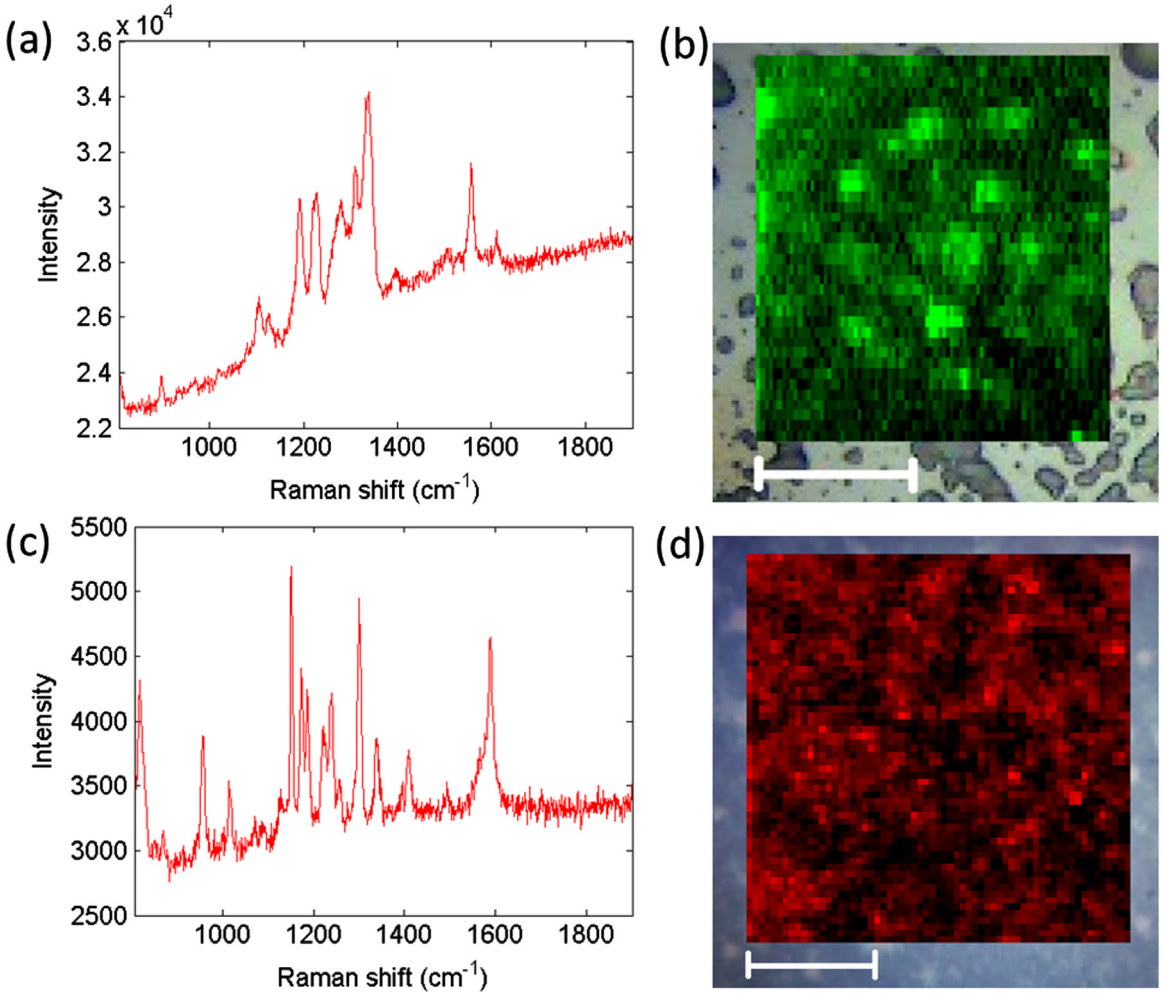


**Fig. 5.** (a) SERS spectrum of 100 pg/ml 3-NT solution on NDG-LSPR chip and (b) shows the corresponding pseudo map of 1335 $cm^{-1}$; (c) SERS spectrum of 1 ng/ml L-tyrosine solution and the corresponding pseudo map of 1590 $cm^{-1}$.

improved the limit of detection to 0.13 pg/ml in PBS, which is four orders of magnitude improvement over reported label-free SPR detection scheme. Thus, our LOD is at the equivalent level of sensitivity reported by conventional gas chromatography – mass spectroscopy but with much less capital investment and running cost. As the linear dynamic range of response extends from pg/ml to ng/ml, we believe it is also practical for early diagnostic of 3-NT biomarkers in clinical applications.

## Acknowledgment

The work described in this article was supported by a grant from City University of Hong Kong (Grant No. 9667110), the National Natural Science Foundation of China (Grant No. 11404192), the Shandong Province Special Grant for High-Level Overseas Talents (Grant No. tshw20120745), the Research Award Fund for Outstanding Young and Middle-aged Scientists of Shandong Province, China (Grant No. BS2014CL002).

## Appendix A. Supporting information

Supplementary data associated with this article can be found in the online version at http://dx.doi.org/10.1016/j.bios.2016.04.017.

## References

Abello, N., Kerstjens, H.A.M., Postma, D.S., Bischoff, R., 2009. J. Proteome Res. 8, 3222–3238.
Ceriello, A., Mercuri, F., Quagliaro, L., Assaloni, R., Motz, E., Tonutti, L., Taboga, C., 2001. Diabetologia 44, 834–838.
Chao, M.-R., Hsu, Y.-W., Liu, H.-H., Lin, J.-H., Hu, C.-W., 2015. Chem. Res. Toxicol. 28, 997–1006.
Ciocca, D.R., Adams, D.J., Bjercke, R.J., Sledge, G.W., Edwards, D.P., Chamness, G.C., McGuire, W.L., 1983. J. Histochem. Cytochem. 31, 691–696.
DeGarmo, E.P., 2003. Materials and Processes in Manufacturing, 9th ed. Wiley, Hoboken, N.J.
Ding, N., Lu, X., Wu, C.-M.L., 2012. Comput. Mater. Sci. 51, 141–145.
Gao, J., Liu, F., Liu, Y., Ma, N., Wang, Z., Zhang, X., 2010. Chem. Mater. 22, 2213–2218.
Georgakilas, V., Otyepka, M., Bourlinos, A.B., Chandra, V., Kim, N., Kemp, K.C., Hobza, P., Zboril, R., Kim, K.S., 2012. Chem. Rev. 112, 6156–6214.
Grace, L.I., Cohen, R., Dunn, T.M., Lubman, D.M., de Vries, M.S., 2002. J. Mol. Spectrosc. 215, 204–219.
Guo, L., Kim, D.-H., 2012. Biosens. Bioelectron. 31, 567–570.
Homola, J., 2008. Chem. Rev. 108, 462–493.
Jin, J., Wang, C., Tao, Y., Tan, Y., Yang, D., Gu, Y., Deng, H., Bai, Y., Lu, H., Wan, Y., 2011. Sens. Actuators B Chem. 153, 164–169.
Lee, S.I., Song, W., Kim, Y., Song, I., Jung, D.S., Jung, M.W., Cha, M.-J., Park, S.E., An, K.-S., Park, C.-Y., 2013. Jpn. J. Appl. Phys. 52, 075101.
Liu, Y., Dong, X., Chen, P., 2012. Chem. Soc. Rev. 41, 2283–2307.
Loo, F.-C., Ng, S.P., Wu, C.-M.L., Kong, S.K., 2014. Sens. Actuators B Chem. 198, 416–423.
Luo, H., Li, H., Fu, Q., Chu, Y., Cao, X., Sun, C., Yuan, X., Liu, L., 2013. Nanotechnology 24, 495702.
Martinez, C.R., Iverson, B.L., 2012. Chem. Sci. 3, 2191.
Mayer, K.M., Hafner, J.H., 2011. Chem. Rev. 111, 3828–3857.
McNay, G., Eustace, D., Smith, W.E., Faulds, K., Graham, D., 2011. Appl. Spectrosc. 65, 825–837.
Mergola, L., Scorrano, S., Del Sole, R., Lazzoi, M.R., Vasapollo, G., 2013. Biosens.

ARTICLE IN PRESS



Bioelectron. 40, 336–341.
Myszka, D.G., 1997. Curr. Opin. Biotechnol. 8, 50–57.
Ng, S.P., Wu, C.-M.L., Wu, S.-Y., Ho, H.-P., Kong, S.K., 2010. Biosens. Bioelectron. 26, 1593–1598.
Ng, S.P., Loo, F.C., Wu, S.Y., Kong, S.K., Wu, C.M.L., Ho, H.P., 2013. Opt. Express 21, 20268–20273.
Ng, S.P., Wu, C.M., Wu, S.Y., Ho, H.P., 2011. Opt. Express 19, 4521–4527.
Ortiz de Montellano, P.R., David, S.K., Ator, M.A., Tew, D., 1988. Biochemistry 27, 5470–5476.
Qiu, G., Ng, S.P., Wu, C.M.L., 2015. Opt. Lett. 40, 1924.
Rajesh, C., Majumder, C., Mizuseki, H., Kawazoe, Y., 2009. J. Chem. Phys. 130, 124911.
Schlücker, S., 2014. Angew. Chem. Int. Ed. 53, 4756–4795.
Shu, L., Vivekanandan-Giri, A., Pennathur, S., Smid, B.E., Aerts, J.M., Hollak, C.E., Shayman, J.A., 2014. Kidney Int. 86, 58–66.
Souza, J.M., Peluffo, G., Radi, R., 2008. Free Radic. Biol. Med. 45, 357–366.
Tohgi, H., Abe, T., Yamazaki, K., Murata, T., Ishizaki, E., Isobe, C., 1999. Neurosci. Lett. 269, 52–54.
Tsikas, D., 2010. Amino Acids 42, 45–63.
Wayenberg, J.-L., Ransy, V., Vermeylen, D., Damis, E., Bottari, S.P., 2009. Free Radic. Biol. Med. 47, 975–982.
Wu, L., Chu, H.S., Koh, W.S., Li, E.P., 2010. Opt. Express 18, 14395.
Xu, W., Xiao, J., Chen, Y., Chen, Y., Ling, X., Zhang, J., 2013. Adv. Mater. 25, 928–933.
Yi, D., Ingelse, B.A., Duncan, M.W., Smythe, G.A., 2000. J. Am. Soc. Mass Spectrom. 11, 578–586.
Zeng, S., Baillargeat, D., Ho, H.-P., Yong, K.-T., 2014. Chem. Soc. Rev. 43, 3426.
Zhang, A., Singh, S.K., Shirts, M.R., Kumar, S., Fernandez, E.J., 2011. Pharm. Res. 29, 236–250.
Zhang, P., Huang, Y., Lu, X., Zhang, S., Li, J., Wei, G., Su, Z., 2014. Langmuir 30, 8980–8989.

Please cite this article as: Ng, S.P., et al., Biosensors and Bioelectronics (2016), http://dx.doi.org/10.1016/j.bios.2016.04.017